Epilepsy Research 155 (2019) 106145

Contents lists available at ScienceDirect

Epilepsy Research

journal homepage: www.elsevier.com/locate/epilepsyres

Altered expression of signaling pathways regulating neuronal excitability in hippocampal tissue of temporal lobe epilepsy patients with low and high seizure frequency

Michael F. Hammer[a,b,*], Ryan Sprissler[a], Robert W. Bina[c], Branden Lau[a], Laurel Johnstone[a], Christina M. Walter[c], David M. Labiner[b], Martin E. Weinand[c,**]

[a] ARL Division of Biotechnology, University of Arizona, Tucson, AZ, USA
[b] Department of Neurology, University of Arizona College of Medicine, Tucson, AZ, USA
[c] Division of Neurosurgery, Department of Surgery, University of Arizona College of Medicine, Tucson, AZ, USA

ARTICLE INFO

Keywords:
Hippocampus
Temporal lobe epilepsy
Seizure frequency
RNA-seq
Pathway analysis

ABSTRACT

Despite recent advances in our understanding of synaptic transmission associated with epileptogenesis, the molecular mechanisms that control seizure frequency in patients with temporal lobe epilepsy (TLE) remain obscure. RNA-Seq was performed on hippocampal tissue resected from 12 medically intractable TLE patients with pre-surgery seizure frequencies ranging from 0.33 to 120 seizures per month. Differential expression (DE) analysis of individuals with low (LSF, mean = 4 seizure/month) *versus* high (HSF, mean = 60 seizures/month) seizure frequency identified 979 genes with ≥2-fold change in transcript abundance (FDR-adjusted p-value ö0.05). Comparisons with post-mortem controls revealed a large number of downregulated genes in the HSF (1676) *versus* LSF (399) groups. More than 50 signaling pathways were inferred to be deactivated or activated, with Signal Transduction as the central hub in the pathway network. While neuroinflammation pathways were activated in both groups, key neuronal system pathways were systematically deactivated in the HSF group, including calcium, CREB and Opioid signaling. We also infer that enhanced expression of a signaling cascade promoting synaptic downscaling may have played a key role in maintaining a higher seizure threshold in the LSF cohort. These results suggest that therapeutic approaches targeting synaptic scaling pathways may aid in the treatment of seizures in TLE.

1. Introduction

Epilepsy is a chronic disorder of the brain that affects approximately 70 million people worldwide (Ngugi et al., 2010). Temporal lobe epilepsy (TLE) is the most frequent form of focal epilepsy in adults, with about 30% of patients resistant to anti-epileptic drugs (AEDs) (Asadi-Pooya et al., 2017). Approximately 30% of refractory cases may opt for a surgical resection, which may include anterior temporal lobectomy with amygalohippocampectomy (ATL/AH) (Tellez-Zenteno and Hernandez-Ronquillo, 2012). However, one in three patients continue with seizures after surgical therapy (Dixit et al., 2016). The etiology of a patient's TLE can vary widely from brain insults such as traumatic brain injury (TBI) to infections, stroke or genetic syndromes. Similarly, the type and frequency of seizures, as well as the age of onset, can be highly variable from patient to patient. Both partial and secondarily generalized seizures occur in TLE patients with generalized tonic-clonic seizures being the most severe and damaging to the neuronal environment (Englot et al., 2013). Thus, there is an urgency to understand the mechanisms of epileptogenesis in order to develop more efficacious treatments.

While it is clear that epileptogenesis involves a disruption of the balance between excitation and inhibition, there is still a large gap in our understanding of how initial seizures begin and how progressive and chronic seizures affect neuronal pathways in the brain. Transcriptomic profiling offers an efficient approach to detect aberrant gene expression patterns in the large number of genes likely to be associated with chronic epilepsy. Many such studies have been performed in animal models of TLE (*e.g.*, (Vieira et al., 2016)). While these studies offer the advantage of access to samples from different regions of the brain and at different stages of epileptogenesis (Hansen et al., 2014), as

* Corresponding author at: ARL Division of Biotechnology, 1657 E Helen Street, Keating 111K University of Arizona, Tucson, AZ, USA.
** Corresponding author at: P.O. Box 245070, 1501 N. Campbell Ave. Tucson, AZ, USA.
E-mail addresses: mfh@email.arizona.edu (M.F. Hammer), MWeinand@surgery.arizona.edu (M.E. Weinand).

https://doi.org/10.1016/j.eplepsyres.2019.05.013
Received 15 January 2019; Received in revised form 17 May 2019; Accepted 23 May 2019
Available online 24 May 2019
0920-1211/ Published by Elsevier B.V.

well as the ability to manipulate the genetics of rodents (McGraw et al., 2017), these models typically involve the use of exogenous agents to evoke seizures (Kandratavicius et al., 2014). There have been several large-scale microarray-based profiling studies comparing the levels of RNA in epileptic *versus* normal human brain tissue. As pointed out previously (Mirza et al., 2015), few of these studies focused on the signaling pathways in which differentially expressed transcripts function. There have been only two reports examining gene expression profiles in brain samples from patients with TLE using the RNA-seq approach, which has many advantages over microarray-based methods. These studies focused on comparing TLE patients with controls or TLE patients with and without hippocampal sclerosis (HS) (Dixit et al., 2016; Griffin et al., 2016).

To date there have been no RNA-seq studies comparing hippocampal tissue from patients with low and high baseline seizure frequency. This is important because differing transcriptional responses may be associated with variation in seizure threshold, and thus provide insights into pathways underlying continued increases or stabilization in seizure frequency (Laxer et al., 2014). Since the concept that "seizures beget seizures" was introduced (Gowers, 1881), there has been an ongoing debate on the extent to which the establishment of seizures themselves can lead to a cascade of physiological processes that culminate in further seizures and synaptic reorganization. Here we perform RNA-Seq on resected hippocampal tissue from adult TLE patients with low and high baseline (pre-surgery) seizure frequency and perform a series of differential expression and pathway enrichment analyses. We find that higher seizure frequency is associated with a greater number of altered signaling pathways relative to controls, many of which are deactivated, and that low seizure frequency in our cohort may be maintained by increased expression of genes affecting synaptic plasticity.

2. Materials and methods

2.1. Tissue samples

The research protocol and consents for all human subjects studied were approved by the University of Arizona Institutional Review Board. Hippocampal tissue was obtained from 12 selected patients diagnosed with medically intractable TLE during anterior temporal lobectomy with amygalohippocampectomy (ATL/AH) (Table 1). The ages of the 9 males and 3 females spanned 16 to 56 years (mean = 32.2yrs) with all patients recording seizure activity for at least 7 years prior to surgery (mean seizure duration = 20.9yrs). The etiology of seizures included drug overdose, traumatic brain injury, meningitis, and febrile seizures, with 8 of unspecified origin. All patients experienced complex partial seizures. A single patient underwent left ATL/AH while the remaining 11 underwent right ATL/AH. The surgical procedure of ATL/AH was a minimum of 5.5 cm right- and a 4.5 cm left-lateral temporal lobe resection. In all patients, the hippocampus was resected *en bloc* posteriorly to at least the level of the cerebral peduncle and preserved for analysis as previously described (Fiala et al., 2013). Pre-surgical seizure frequency data were collected for each patient, which ranged from 0.33 to 120 seizures per month. Patients were followed clinically for 5–94 months post-operatively (mean = 37mos).

Table 1
Clinical characteristics of patients with refractory temporal lobe epilepsy (TLE).

Subject #	Sex	Age (yr)	Duration (yr)	Seizures/mo	HS	Etiology	Onset age (yr)
1	F	32	8	0.33	*	CVA	24
2	M	16	10	4	+	Unk	6
3	M	32	17	4	*	Unk	15
4	M	32	29	4	−	Unk	3
5	M	30	8	4	+	OD	22
6	M	21	Unk	8	+	Unk	Unk
7	F	31	16	8	+	Unk	15
8	M	38	37	10	−	Feb	1
9	F	41	21	20	+	Unk	20
10	M	38	33	30	+	Unk	5
11	M	19	7	60	+	TBI	12
12	M	56	44	120	+	Men	12

Duration = duration of seizures prior to surgery; SZ freq/mo = frequency of seizures per month prior to surgery; CVA = stroke; OD = drug overdose; TBI = traumatic brain injury; Men = meningitis; Feb = febrile seizures.
HS = hippocampal sclerosis (* indicates hippocampal atrophy) based on preoperative MRI scan.

2.2. RNA-seq

RNA was isolated and initial QC assessed. Libraries were constructed using a stranded mRNA-Seq Kit and average fragment size was assessed. After concentrations were determined with an adaptor-specific qPCR kit, equimolar samples were pooled and clustered for sequencing on the HiSeq2500 (Illumina). Sequencing was performed using Rapid-Run SBS 2 × 100bp chemistry (Illumina). RNA-seq data from controls came from five healthy post-mortem human hippocampal tissues (Hwang et al., 2016). Sample data were demultiplexed, trimmed and quality filtered, and Fastq files were splice aligned against the GRCh37 reference genome using STAR aligner version 2.5.2b (Dobin et al., 2013). Gene expression counts were obtained using htseq-count version 0.6.1 (Anders et al., 2015). Both splice alignment and counting were performed with Ensembl Annotation of the NCBI reference genome and raw counts analyzed with edgeR version 3.16.5 (Robinson et al., 2010). Correlation patterns between protein coding genes were calculated using weighted gene co-expression analysis R package, version 1.66 (Langfelder and Horvath 2008) (see supplementary information).

2.3. Differential expression analysis

Differential expression (DE) analysis was performed on two groups of 3 subjects at the extreme ends of the pre-surgery seizure frequency distribution: 3 males with low seizure frequency (LSF group: 4 seizures/month) and 3 males with high seizure frequency (HSF group: 30, 60 and 120 seizures/month). The DE analysis utilized edgeR's exactTest function, which uses Benjamin-Hochberg correction to compute an upper bound for the expected FDR. Gene expression counts were first normalized using the calcNormFactors function, which uses the trimmed mean of M values (TMM) to create a set of scaling factors that eliminates composition biases between sample libraries. Due to the variance between samples, the trended dispersion (the dispersion calculated from a gene's abundance) was used for the exactTest calculation. We performed principal component analysis (PCA) using DESeq2's plotPCA function on a set of log2-transformed counts calculated by the rlog function in DESeq2 (Love et al., 2014). PCA plots were generated based on read counts for the 500 genes with the greatest variance in expression.

2.4. Quantitative reverse transcriptase polymerase chain reaction (qRT-PCR)

cDNA was generated from hippocampal RNA samples with the SuperScript III kit (Life Technologies). Taqman probes were obtained from Life Technologies for the genes *ARC*, *CACNA1C*, *CAMK2A*, *ERBB3*, *FOSL2*, *GLDN*, *GRIA1*, *GRIA2*, *NPTXR*, *PRKCE*, and *SRF*. Taqman reactions were performed in 15 u l reaction volumes using the Taqman Fast Advance Master Mix. RT-PCR reactions were performed comparing HSF samples *versus* LSF samples as we did not have RNA from controls. All reactions were run in triplicate on an ABI 7900 H T using the SDS 2.4 software (Life Technologies) with ABI384 well Optical PCR plates and AB-1170 Optical PCR film (Fisher Scientific). All samples were run with

the endogenous control GAPDH probe set (Life Technologies #Mm99999915_g1). Differential expression analysis was performed using the standard delta-delta CT method (Livak and Schmittgen, 2001).

2.5. Pathway-enrichment analysis

We performed Gene Set Enrichment Analysis v3.0 (Subramanian et al., 2005) to infer enriched Reactome and KEGG gene-sets based on the up- or downregulated genes identified in the LSF and HSF *versus* control samples. Enrichment Map (Merico et al., 2010) tool was used to determine the connections between enriched pathways by identifying functionally coherent gene-sets (*i.e.*, pathways) that are statistically over-represented in a given gene list. We employed an overlap coefficient cut-off of 0.25—two pathways were deemed connected only if the ratio of the size of the intersection over the size of the smallest pathway was 0.25 or more. The Network Analyzer tool was used to calculate network parameters, including 'closeness centrality' of nodes. We followed the commonly employed strategy (Mirza et al., 2015) to filter out the broadest functional category (*i.e.*, the top hierarchy of biological processes in Reactome) when ranking the most statistically significant pathways.

2.6. Ingenuity pathway analysis

Pathway analysis was performed using Qiagen's Ingenuity Pathway Analysis (IPA) software. The differential expression results from edgeR were filtered based on logFC (cutoff 1.0), p-value (≤ 0.05) and FDR (≤ 0.05). This filtered list was enriched for pathways utilizing IPA's "core analysis" function, using logFC in order to calculate pathway directionality (z-scores). IPA uses two scores that address two independent aspects of inference: an 'enrichment' score [Fisher's exact test (FET) P-value] that measures overlap of observed and predicted regulated gene sets, and a z-score assessing the match of observed and predicted up/down regulation patterns. A z-score is well-suited for this kind of problem because it serves as both a significance measure and a predictor for the activation state of the pathway (Kramer et al., 2014). We also performed upstream regulator analysis in IPA, which identifies molecules upstream of the genes in the dataset that potentially explain the observed expression changes.

3. Results

3.1. Patient phenotypes and principal component analysis

The pre-surgery seizure frequency of our 12 patients ranged from 0.33 to 120 seizures per month (Table 1). While there was a trend for patients with higher seizure frequency to also have hippocampal sclerosis (HS), there were four 'low seizure frequency' patients exhibiting HS (n = 2 with 4 seizures/mo and n = 2 with 8 seizures/mo), and one patient with 10 seizures/mo that did not exhibit HS. Approximately 20 million high quality sequencing reads were obtained per sequencing run, and > 90% of these reads aligned to the reference genome. All reads were considered for analysis, leading to a final set of 63,677 transcripts for differential expression analysis.

Fig. 1**A** shows the results of a principal component analysis that was conducted with the 500 transcripts with the greatest variance to determine the largest source of variation in the data. The first two principal components explain ~61% of the total variation in gene expression. The high seizure frequency (HSF) subjects cluster tightly on the left and right side of the plot, while the low seizure frequency (LSF) subjects are spread across the upper central to lower right side of the plot. Two subjects appear to represent exceptions to this pattern (#5 and #9).

We then performed a similar analysis after including RNA-seq data from five "controls" that derive from five adult autopsy samples from hippocampal tissue (Hwang et al., 2016). We limited the analysis of our data to the three males with the lowest seizure frequencies (all with 4 seizures/mo), and the three male subjects with the highest seizure frequencies (*i.e.*, 30, 60, and 120 seizures/mo). The first two principal components explain 77% of the gene expression variation (Fig. 1B). Again the HSF subjects tightly cluster on the left side while the LSF subjects are positioned on the right side on the perimeter of the five control samples. These results suggest that seizure frequency is one of the main determinants of variance within expression data.

3.2. Differential expression (DE) analysis

Initially, we performed DE analysis on the aforementioned LSF *versus* HSF groups. In our data, 979 transcripts were identified with a $\geq$2-fold difference in abundance (FDR-adjusted p-value < 0.05), 722 of which had higher abundance in the LSF group and 257 had higher abundance in the HSF group (Table S1). We then examined a set of genes that are expressed in the human brain during postnatal and adult developmental stages, and that are differentially expressed in each of four brain regions (cerebellar cortex, mediodorsal nucleus of the thalamus, striatum, and hippocampus) (Kang et al., 2011). As predicted, we found that the hippocampus exhibited the largest percentage of differentially expressed genes (DEGs) in comparisons between the LSF and HSF groups (*e.g.*, 47% *versus* 13–26% for the other 3 brain regions). The same pattern held when we examined each brain region at four developmental stages: prenatal, prenatal/postnatal, postnatal, and postnatal/adult stages. The hippocampus exhibited the highest percentage of DEGs in all four stages (data not shown). To test for hidden bias, we performed the same DE analysis on two "mixed" seizure frequency groups, each consisting of a low, a medium and a high seizure frequency subject (LMH) (*i.e.*, individuals 2, 6 and 10 *versus* 3, 8, and 11 in Table 1). We identified only 15 genes with $\geq$2-fold differences in transcript abundance (FDR-adjusted p-value < 0.05).

We then performed DE analysis comparing the RNA-seq data from the five controls with each of our LSF and HSF groups. In the LSF *versus* control comparison we identified 399 significantly downregulated and 834 significantly upregulated transcripts ($\geq$2-fold difference in abundance, FDR-adjusted p-value < 0.05) (Fig. 2**A;** Table S2). The comparison with the HSF group revealed a greater number of DEGs: 1676 and 1314 transcripts significantly down- and upregulated, respectively ($\geq$2-fold difference in abundance, FDR-adjusted p-value < 0.05) (Table S3). Fig. 2**B** shows the overlap in DEGs between the two seizure frequency groups: 525 of the 1617 upregulated transcripts (31.9%) and 344 of the 1725 downregulated transcripts (19.9%) are shared. On the other hand, with respect to the downregulated genes, only 54 (3.1%) are unique to the LSF group compared with 1327 (76.9%) that are unique to the HSF group. Unique upregulated genes comprise 20.3% (304) and 47.8% (788) of the total for the LSF and HSF groups, respectively. This illustrates the large fraction of downregulated transcripts that are unique to the HSF group and the relatively small fraction of DEGs (especially those that are downregulated) that are unique to the LSF group.

To check the similarity of comparisons involving RNA-seq data based solely on our samples and data based on comparisons with autopsy controls, we counted the number of shared DEGs in each comparison (Fig. 2C). Of the 979 DEGs in the HSF *versus* LSF comparison, 70% and 13% were shared with the HSF *versus* Control and LSF *versus* Control comparisons, respectively. A total of 22 DEGs (22.6%) were found only in the HSF *versus* LSF comparison. When we compare the top 10 DEGs with lower transcript abundance in HSF relative to LSF, we note that 6 of these were actually downregulated in HSF *versus* controls, while 3 were upregulated in LSF *versus* controls. In the top 10 DEGs with higher transcript abundance in HSF relative to LSF, 9 were actually upregulated in HSF *versus* controls (data not shown).

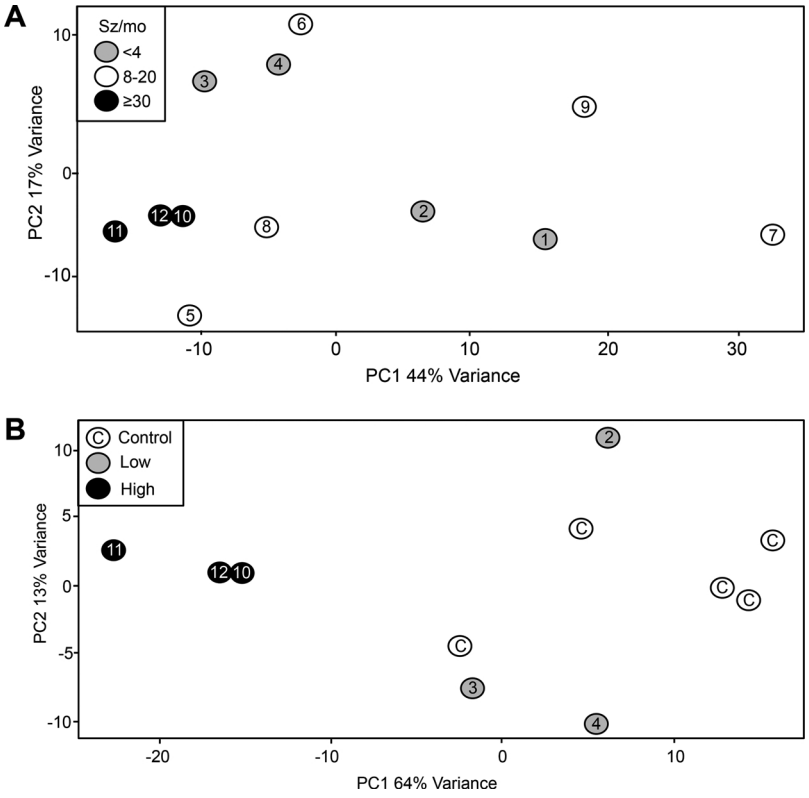

Fig. 1. Principal component analysis. **A**) PCA based on the 500 transcripts with the greatest variance in expression. Numbers in circles refer to patient numbers in Table 1. Gray circles, open-circles and black circles refer to monthly seizure frequencies of < 1-4, 8–20, and ≥30, respectively. The first two principal components explain ˜61% of the total variation in gene expression. **B**) PCA including 5 post-mortem control samples based on the 500 transcripts with the greatest variance in expression. Gray, black and open (with C) circles refer to LSF, HSF, and controls, respectively. The first two principal components explain 77% of the variance in transcript abundance.

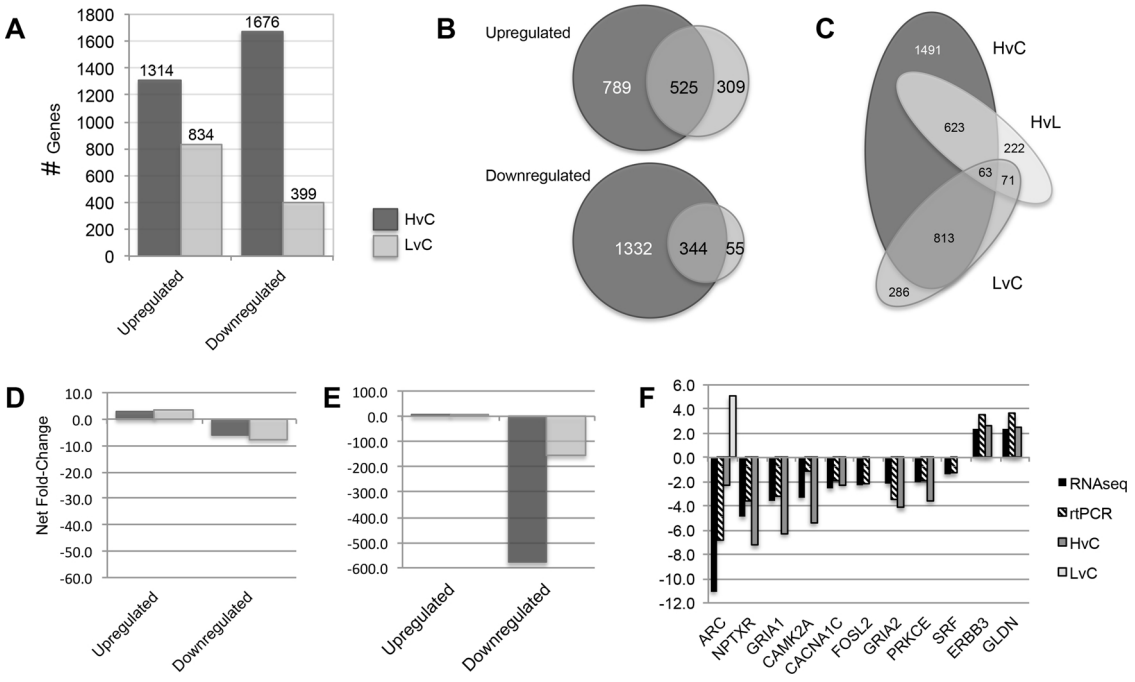

Fig. 2. Differential gene expression between HSF *versus* LSF patients, and between HSF patients *versus* controls and LSF patients *versus* controls. A) Number of upregulated and downregulated differentially expressed genes (DEGs) in the HSF and LSF relative to controls. B) Number of shared and unique upregulated and downregulated DEGs in comparisons between HSF and LSF relative to controls. C) Number of DEGs in comparison between HSF and LSF (HvL), and sharing of DEGs among all three comparisons (HvC, LvC, and HvL). D) Mean fold-change (i.e., net fold-change/number of DEGs) for upregulated and downregulated shared between LSF and HSF in comparisons relative to controls. E) Mean fold-change for upregulated and downregulated DEGs that are unique to LSF and HSF groups in comparisons relative to controls. F) Confirmation of selected RNA-seq data by qRT-PCR. Taq-man assays were carried out as described in Methods. RNAseq and rtPCR columns represent the ratio of transcript abundance in HSF relative to LSF, while HvC and LvC represent HSF and LSF groups relative to controls.

3.3. Mean fold-change in transcript abundance

Fig. 2 shows the mean fold-change in transcript abundance (*i.e.*, net fold-change/#genes) for the LSF and HSF groups relative to controls, both for gene sets that are unique to the LSF and HSF group (Fig. 2D) and for the gene sets that are shared by both groups (Fig. 2E). The mean fold-changes in transcript abundance for the genes that are unique to the LSF and HSF groups are similar for both the upregulated (FC: +3.8 and +3.0, respectively) and the downregulated gene sets (FC: −7.8 and −5.8, respectively) (Fig. 2D). This pattern holds for the shared upregulated gene set, which indicates that transcript abundance is increased by an average of 5.0- and 5.3-fold for the LSF and HSF groups, respectively. On the other hand, there is a much larger effect size for the downregulated genes in the HSF group, which show an average drop in transcript abundance of almost 580-fold *versus* 155-fold for the shared downregulated LSF genes (note different scales in Fig. 2**D** and **E**).

3.4. Confirmation of quantitative changes by qRT-PCR

Eleven transcripts with altered abundance in the RNA-seq data were subjected to confirmation by qRT-PCR, including genes with both high and low constitutive expression: *ARC*, *CACNA1C*, *CAMK2A*, *ERBB3*, *FOSL2*, *GLDN*, *GRIA1*, *GRIA2*, *NPTXR*, *PRKCE*, and *SRF*. The predicted differences between HSF and LSF individuals were confirmed for these 11 transcripts (Fig. 2F), with excellent concordance between RNA-seq and qRT-PCR for all 11 genes (Pearson correlation coefficient: $r = 0.924$, $p = 4.8 \times 10^{-5}$). Note that there is increased expression of ARC in the LSF relative to controls, and decreased expression in HSF *versus* controls.

3.5. Network and pathway enrichment analysis

To visualize relationships among significantly enriched gene sets and to identify centrally located pathways within sub-networks, we performed gene set enrichment analyses based on the upregulated and downregulated DEGs identified in HSF *versus* LSF, and LSF and HSF *versus* controls. The gene enrichment map for HSF *vs* LSF shown in Fig. S1 has 52 nodes; however, only 10 of these had a p-value ≤0.05. The most significant Reactome superpathways include Metabolism, Neuronal System and Developmental Biology. Within these top-level groups the most significant pathways include Metabolism of Lipids, Class A1 Rhodopsin-like receptors, and Axon Guidance, as well as the KEGG pathway, *Cell Adhesion Molecule Cams*. Signal transduction was the most central node in the network, with *Calcium* and *MAPK Signaling* being the two most statistically significant KEGG pathways, and *GPCR Ligand Binding* being the most significant Reactome pathway within the Signal Transduction superpathway. Metabolism and Cell Adhesion are the only pathways that appear to be more highly enriched (activated) in the HSF *versus* LSF, while the opposite is true for almost all other pathways, including the pathways in Neuronal System and Signal Transduction.

For the comparisons between the two seizure groups and controls, we initially created separate networks for the LSF and HSF gene sets that passed very permissive thresholds in the enrichment analysis (*i.e.*, p ≤ 1.0 and FDR q-value≤ 1.0). This allowed us to visualize relationships among all pathways (*i.e.*, gene sharing) with positive or negative enrichment scores. This analysis revealed a highly interconnected network of 228 pathways, with an average of 13.2 links among all nodes (data not shown). Closeness centrality network analysis identified 'Signal transduction' as the most central 'hub' pathway (centrality index = 0.578), which also has the largest number of links to other nodes (n = 147).

We then constructed a combined network showing the Enrichment Map gene-sets that passed a more stringent threshold (*i.e.*, p-value < 0.05, False Discovery Rate (FDR) < 25%). Fig. 3 shows this network with 51 significantly enriched gene sets (out of > 2000 in the Reactome knowledge base): 40 are specifically enriched in HSF, 9 are specific to LSF, and 2 are enriched in both seizure frequency groups. These 51 pathways fall within 14 top-level Reactome superpathways. The top-ranked pathways identified in HSF and LSF are annotated by numerical rank on the enrichment map. Four of the top-ranked gene sets enriched in the HSF are within *Signal Transduction*, 3 within *Neuronal System*, and 2 within *Disease*, while 4 of the top-ranked LSF gene sets are within *Immune System*, and 2 are within *Gene Expression*. Consistent with the DE results presented above, enrichment analysis reveals that nearly all of the significant HSF gene sets have a negative enrichment score (*i.e.*, blue color in Fig. 3, higher enrichment in control relative to HSF): 11/11 in *Neuronal System*, 7/7 in *Signaling Transduction (GPCR)*, 7/7 in *Extracellular Matrix Organization*, 3/6 in *Transport of Small Molecules*, 3/5 in *Metabolism of Proteins*, and 3/3 in *Muscle Contraction*. Eleven enriched gene sets in Fig. 3 have positive enrichment scores, 9 of which are specific to the LSF group and falling within *Immune System*, *Gene Expression*, and *Signal transduction*.

To confirm and extend these results, we used Ingenuity Pathway Analysis (IPA) to predict the activation state of significantly altered pathways based on the distinct up- and down-regulation pattern of the DEGs. Table 2 lists the activation states of 34 pathways that met the dual criteria of a z-score value ≥2.0 (score based on the number of loci in the pathway that are differentially expressed in the direction consistent with predictions of an activated state of the pathway) and p-value ≤0.05 (number of loci that are significantly differentially expressed relative to the total number of loci in the pathway). We categorized these pathways into five more general (non-mutually exclusive) functional classes: *Immune System*, *Second Messenger Signaling*, *Neuronal System*, *Nuclear Receptor Signaling*, and *Cellular Growth and Development*. Pathways could be characterized as 'Shared Activated' and 'Shared Deactivated' (*i.e.*, activated or deactivated in both LSF and HSF), LSF Activated or Deactivated (*i.e.*, activated or deactivated in LSF only), and HSF Activated or Deactivated (*i.e.*, activated or deactivated in HSF only) (Fig. 4). Of the 34 pathways, nearly half (n = 16) were HSF deactivated, while none was LSF deactivated.

Pathway activation states are not evenly distributed among functional categories. For instance, *Immune System* pathways comprise 100% of the Shared Activated category and make up the majority of LSF and HSF activated pathways (Fig. 4). On the other hand, *Signal Transduction* and *Neuronal System* pathways are mostly found in the HSF Deactivated category, (*i.e.*, 10/14 and 5/6 of the total in each, respectively), making up ˜70% of the pathways in this category.

The most statistically significant pathways in Table 2 are HSF Deactivated within *Neuronal System* and include Opioid Signaling, Synaptic Long-Term Depression and Long-Term Potentiation, and Neuropathic Pain Signaling in Dorsal Horn Neurons. Additional key HSF Deactivated pathways are in *Second messenger Signaling*, including Calcium Signaling, Dopamine-DARPP32 Feedback in cAMP Signaling, and CREB Signaling. Opioid Signaling and Gβγ Signaling are the only pathways with significantly positive and negative z-scores in LSF and HSF, respectively (Fig. 4). Secondarily, the *Immune System* pathways IL-6 and HMGB1 Signaling, both Shared Activated, were strongly enriched, as were the HSF Deactivated eNOS Signaling and CCR4 Signaling in Macrophages.

Similar results were found when we compared HSF with LSF, with 16 of the 26 significantly altered pathways shared with the analyses based on comparisons with controls (Table S4). All but two pathways were HSF deactivated, and 12 of 26 were within the Neuronal System category. Of the 10 pathways that were unique to this analysis, 4 were in Neuronal System, 2 within Second Messenger signaling, 1 in Immune System, and 3 in other categories (Cardiovascular signaling and Cellular Growth and Development).

4. Discussion

We have employed next generation approaches to sequence

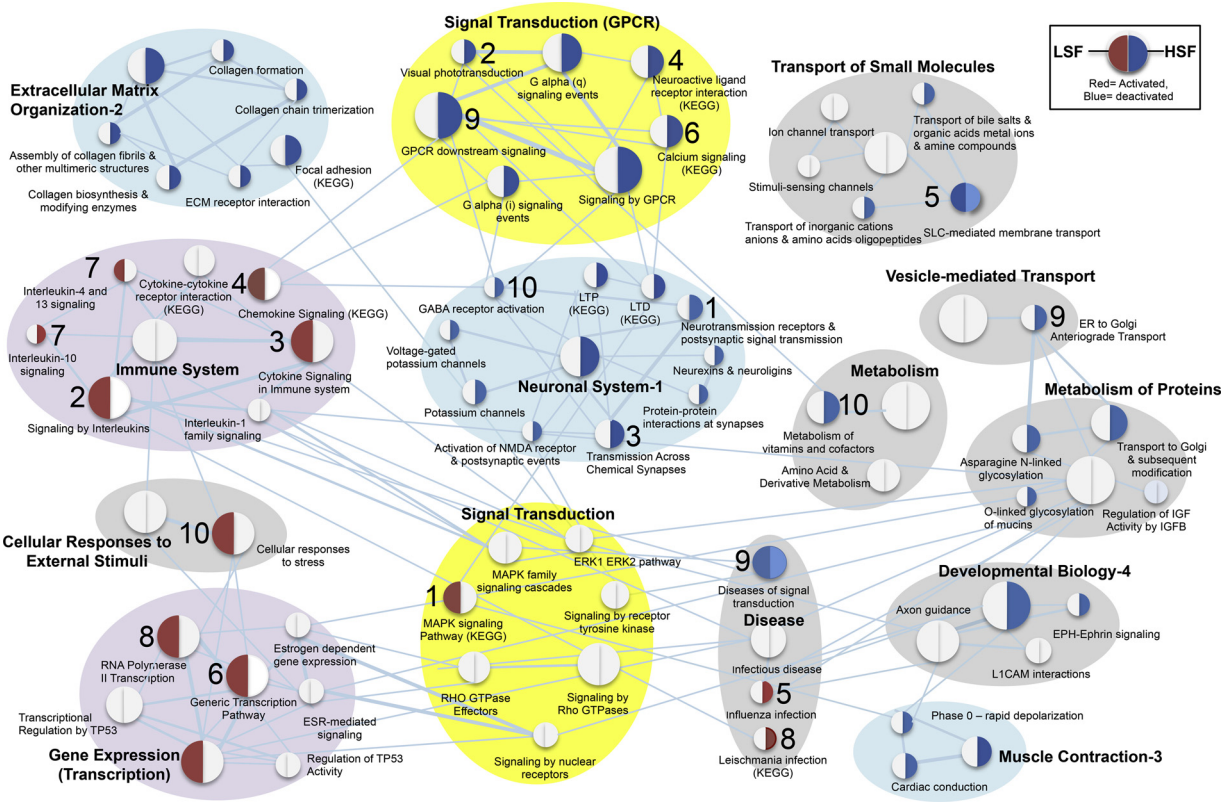

Fig. 3. Gene enrichment map for gene sets showing positive and/or negative enrichment in LSF and HSF *versus* controls. Gene-set enrichment results were graphically mapped to the Enrichment Map (Merico et al. 2013). Nodes are arranged so that highly similar gene-sets are placed close together; these clusters are related to biological functions. Node size represents the number of genes in the gene-set; edge thickness is proportional to the overlap between gene-sets. The enrichment score is mapped to the node where node color ranges from red (high enrichment in LSF or HSF) to white (no enrichment) to blue (high enrichment in the control relative to LSF or HSF). The left side of the node represents enrichment in the LSF and the right side indicated enrichment in the HSF *versus* controls. Colors are shown only for nodes that had p-values ≤ 0.05 and FDR ≤ 0.25, while nodes without colors were mapped based on a lower stringency analysis (p-values ≤0.1 and FDR ≤ 1.0). Numbers to the left or right of nodes indicate p-value rank order for that gene set in the LSF *versus* controls and HSF *versus* controls, respectively. Background color of cluster indicates trend toward activation of supercluster (light lavender), deactivation of supercluster (light blue), or supercluster inferred to be central hub of entire network (light yellow).

transcripts present in resected hippocampal tissue from patients with low and high pre-surgery seizure frequencies to infer the molecular mechanisms involved in the onset and propagation of seizures. To our knowledge no previous gene expression study has subdivided TLE patients into different seizure frequency groups. This strategy allowed us to identify expression patterns that distinguish TLE patients from non-epilepsy individuals, as well as to explore differences related to seizure frequency within a TLE patient cohort. This resulted in a large number of genes that significantly differed in transcript abundance between the LSF and HSF groups. Perhaps this is not surprising given the extent of difference in monthly seizure frequency in the two groups, and the length of time our patients experienced medically intractable seizures (Table 1).

We employed two different approaches to interpret our transcriptome data in terms of prior biological knowledge. Our gene enrichment results for the HSF cohort are similar to those in Mirza et al.'s (2015) microarray-based expression study in which we find 5 of the 10 most significantly enriched Reactome pathways in the *Neuronal System* superpathway, as well as shared enriched gene sets in *Signal Transduction* and *Transport of Small Molecules* (Table 3). In contrast, our LSF cohort differed, with the 10 most significantly enriched Reactome pathways clustering in *Immune System*, *Gene Expression*, and *Cellular Responses to External Stimuli* (Table 3). Similar to Mirza et al. (2015) we found *Signal Transduction* (0.609, degrees = 22) to be the most centrally located hub pathway in the LSF network, while *Cellular Responses to External Stimuli* (Cellular Senescence: 0.353, degrees = 29) was the most centrally located pathway in the HSF network, followed closely by *Disease* (0.331, degrees = 30). Thus, our results predict different influential pathways contributing to the HSF and LSF phenotypes. When we perform centrality closeness analysis on the combined network in Fig. 3 we find that *Signal Tranduction* (0.578, degrees = 147) is the most centrally located hub. This superpathway is divided into two major clusters of nodes: one with several closely related G-protein couple receptor pathways that are connected with *Neuronal System* nodes, and a second cluster of highly interconnected *Signal Transduction* gene sets with links to Immune System, Transcription, Disease, Metabolism of Proteins, and other developmental processes (Fig. 3). Many of the signaling pathways identified here are activated by GPCRs, including: the ERK/MAPK pathway, CREB Signaling, Calcium Signaling, Opioid Signaling, G-protein-gated ion channels including calcium channels, and G-protein-gated inwardly rectifying potassium channels.

We also made use of the algorithms and knowledge base in Ingenuity Pathway Analysis (IPA), which is a more powerful approach than gene-set enrichment because it leverages knowledge about the direction of effects rather than mere associations (Kramer et al., 2014). These different methods produced highly consistent results, generating a cohesive picture that is characterized by 1) widespread deactivation of multiple signaling pathways with roles in a variety of biological processes in the HSF group, and 2) a much smaller number of pathway alterations in the LSF group, mainly in the areas of Immune System, Second Messenger Signaling, and Transcription. In the following sections we consider pathways that are uniquely activated or deactivated in the LSF and HSF groups and explore the possibility that alterations in these pathways are the cause or consequence of differences in seizure

Table 2
Statistically enriched[1] canonical pathways identified by IPA in the HSF and LSF versus contols comparisons.

	LSF vs Ctr			HSF vs Ctr				
	# genes	p value	z score	# genes	p value	z score	#genes	Predicted State
Immune System								
IL-6 Signaling	16	1.20×10^{-3}	2.00	35	8.21×10^{-6}	2.20	128	Shared Activated
HMGB1 Signaling	15	4.57×10^{-3}	2.67	31	6.12×10^{-4}	2.56	133	Shared Activated
TNFR2 Signaling	6	4.31×10^{-3}	2.00	9	1.06×10^{-2}	2.12	30	Shared Activated
TNFR1 Signaling	8	4.44×10^{-3}	2.65	11	4.89×10^{-2}	2.11	50	Shared Activated
p38 MAPK Signaling	10	*0.104*	3.00	26	4.69×10^{-3}	2.29	120	HSF Activated
Acute Phase Response Signaling	19	1.70×10^{-3}	*1.29*	36	1.54×10^{-3}	2.19	170	HSF Activated
Toll-like Receptor Signaling	10	6.60×10^{-3}	*1.41*	19	2.83×10^{-3}	2.00	76	HSF Activated
Dendritic Cell Maturation	16	5.08×10^{-3}	*0.26*	39	2.47×10^{-3}	2.14	193	HSF Activated
Th1 Pathway[2]	7	*1.000*	*−0.82*	25	3.64×10^{-2}	2.24	135	HSF Activated
IL-8 Signaling	17	3.28×10^{-2}	2.84	47	5.51×10^{-5}	*1.77*	197	LSF Activated
IL-17A Signaling in Gastric Cells	6	1.61×10^{-3}	2.24	7	3.35×10^{-2}	*0.38*	25	LSF Activated
Aryl Hydrocarbon Receptor Signaling[2]	14	1.75×10^{-2}	2.53	24	*0.089*	*0.94*	141	LSF Activated
iNOS Signaling	6	3.03×10^{-2}	2.24	10	*0.055*	2.33	45	LSF Activated
eNOS Signaling	11	*0.303*	*—1.27*	40	1.15×10^{-4}	—3.09	172	HSF Deactivated
CCR5 Signaling in Macrophages	7	*0.238*	—	29	4.66×10^{-6}	—2.11	95	HSF Deactivated
UVC-Induced MAPK Signaling	2	*1.00*	—	12	6.41×10^{-3}	—2.11	43	HSF Deactivated
GP6 Signaling Pathway	11	*0.099*	—2.11	34	5.92×10^{-5}	—3.09	134	HSF Deactivated
Second Messenger Signaling								
Gαi Signaling	13	1.10×10^{-2}	2.71	32	3.39×10^{-5}	*0.54*	120	LSF Activated
cAMP-mediated signaling	20	1.80×10^{-2}	3.44	58	1.42×10^{-7}	*—0.96*	227	LSF Activated
p38 MAPK Signaling	10	*0.104*	3.00	26	4.69×10^{-3}	2.29	120	HSF Activated
ERK5 Signaling	5	*0.270*	2.24	14	3.81×10^{-2}	2.50	66	HSF Activated
G Beta Gamma Signaling	5	*1.00*	2.00	31	2.96×10^{-5}	—2.34	114	HSF Deactivated
Calcium Signaling	12	*0.409*	*1.27*	68	4.18×10^{-14}	—4.24	206	HSF Deactivated
GPCR-Mediated Nutrient Sensing in Enteroendocrine Cells[2]	9	*0.139*	*1.67*	34	8.43×10^{-7}	—2.40	112	HSF Deactivated
Dopamine-DARPP32 Feedback in cAMP Signaling[2]	11	*0.252*	*0.71*	35	1.54×10^{-3}	—3.43	164	HSF Deactivated
Gαs Signaling	6	*0.529*	*1.00*	21	3.89×10^{-2}	—2.68	110	HSF Deactivated
Neuronal System								
Cholecystokinin/Gastrin-mediated Signaling	13	2.57×10^{-3}	2.50	33	1.83×10^{-7}	*0.52*	101	LSF Activated
Opioid Signaling	16	*0.213*	2.67	69	5.94×10^{-11}	—3.05	242	HSF Deactivated
Synaptic Long Term Depression	8	*1.00*	*0.71*	46	9.63×10^{-7}	—4.13	174	HSF Deactivated
CREB Signaling in Neurons[2]	10	*1.00*	*0.45*	52	2.31×10^{-6}	—3.18	212	HSF Deactivated
Synaptic Long Term Potentiation	7	*0.469*	*0.38*	32	4.83×10^{-5}	—3.65	122	HSF Deactivated
Neuropathic Pain Signaling In Dorsal Horn Neurons	8	*0.264*	*0.71*	34	1.65×10^{-6}	—3.77	115	HSF Deactivated
Huntington's Disease Signaling	11	*1.00*	*—1.00*	45	1.13×10^{-2}	—2.04	250	HSF Deactivated
GPCR-Mediated Nutrient Sensing in Enteroendocrine Cells[2]	9	*0.139*	*1.67*	34	8.43×10^{-7}	—2.40	112	HSF Deactivated
Dopamine-DARPP32 Feedback in cAMP Signaling[2]	11	*0.252*	*0.71*	35	1.54×10^{-3}	—3.43	164	HSF Deactivated
Nuclear Receptor Signaling								
PPAR Signaling	14	4.62×10^{-4}	—2.14	24	7.29×10^{-4}	—2.86	95	Shared Deactivated
Androgen Signaling	8	*0.440*	2.00	33	2.90×10^{-4}	—2.60	137	HSF Deactivated
Aryl Hydrocarbon Receptor Signaling[2]	14	1.75×10^{-2}	2.53	24	*0.089*	*0.94*	141	LSF Activated
Cellular Growth and Development								
Th1 Pathway[2]	7	*1.00*	—0.82	25	3.64×10^{-2}	2.24	135	HSF Activated
CREB Signaling in Neurons[2]	10	*1.00*	0.45	52	2.31×10^{-6}	—3.18	212	HSF Deactivated

[1]Only pathways with p-values ≤ 0.05 and z-scores ≥ 2.0 are considered statistically significant. Non-significant values are italicized and in the case of p-values are written as decimals.
[2]Present in more than a single biological category.

frequency.

4.1. Divergent patterns of gene expression associated with differences in seizure frequency

Visual inspection of Fig. 3 reveals a striking difference in gene set enrichment between LSF and HSF groups. Of the 40 gene sets that were significantly enriched solely in the HSF group, 38 show a pattern of negative enrichment score, while gene sets that were uniquely enriched in the LSF all had positive enrichment scores. The IPA results also reveal major differences between seizure frequency groups with respect to pathway activation/deactivation (Table 2, Fig. 4). In this section, we focus on those pathways that are uniquely activated/deactivated in each group.

Numerous studies have suggested a role for inflammation associated with innate immunity in epileptogenesis and the development of pharmacoresistance in mesial TLE (mTLE) (Vieira et al., 2016). Indeed several inflammation-signaling pathways were similarly altered in both the HSF and LSF groups (Table 2). On the other hand, IL-8, IL-17A and iNOS pathways are exclusively activated in the LSF, while Th1, Acute Phase Response, and Dendritic Cell Maturation are exclusively activated in the HSF. Th1 cells promote cell-mediated immune response and produce IFN-γ, IL-2, and tumor necrosis factor-β, and have been shown to play an important role during the acute phase of the pathogenesis of mumps parotitis (Malaiyan et al., 2016). The acute phase response is a rapid inflammatory response that provides initial protection against damage from tissue injury, including sterile inflammation triggered by seizures (Vezzani et al., 2016). A related HSF activated pathway involves the maturation of dendritic cells, which are known to increase in number during neuroinflammation and to be recruited to the brain from the periphery after induction of seizures in a rat model of TLE (Li et al., 2013).

Notably, more than half of all differentially altered pathways fall into the HSF-deactivated category (Table 2, Fig. 4), of which Calcium Signaling is inferred to be the most strongly deactivated. Calcium signaling is increasingly recognized as an important factor in

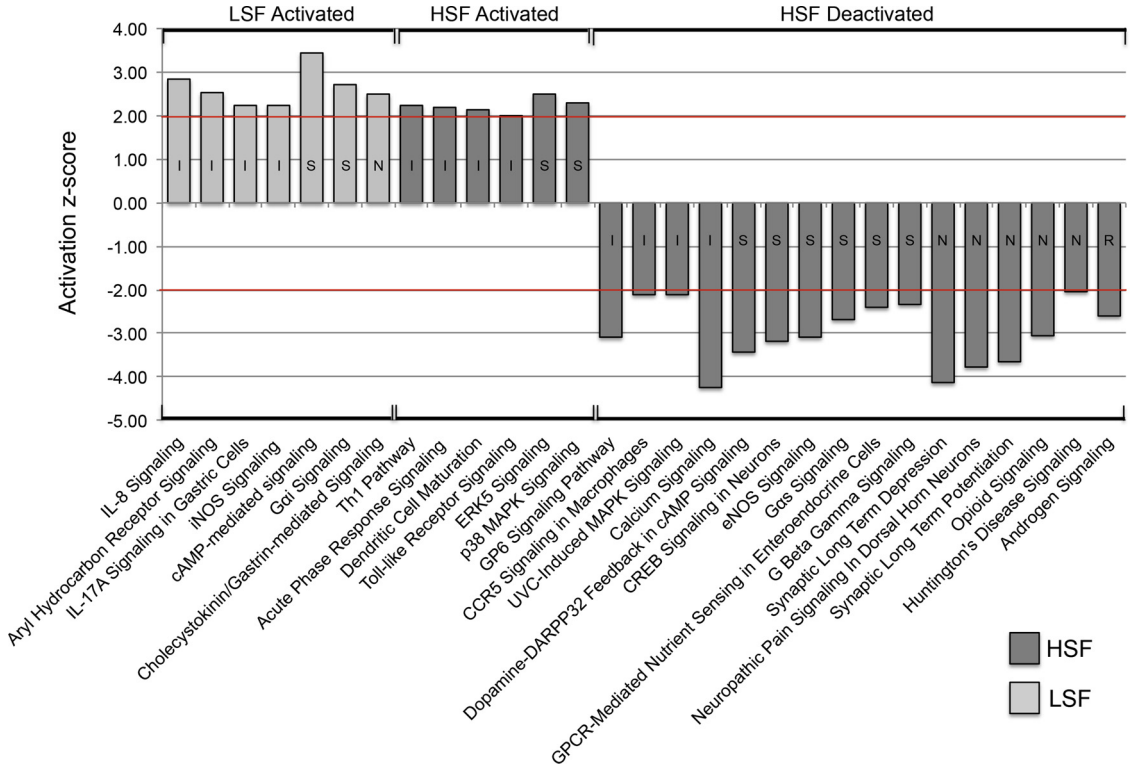

Fig. 4. Ingenuity Pathway analysis of DEGs in LSF and HSF *versus* controls. The 29 pathways in Table 2 that were differentially activated in the LSF and HSF and that passed the dual threshold of significant p-value ($p < 0.05$) and z-score (≤ -2.0 or $\geq +2.0$) are shown. Only the activation z-scores are depicted (*i.e.*, with bars). The pathways are grouped according to their predicted activation state in HSF and LSF. The red horizontal lines indicate statistical significance by z-score. (Dark gray bars = HSF, light gray bars = LSF). Letters on bars stand for I = Immune System; S = Second Messenger Signaling; N = Neuronal System; R = Nuclear Receptor Signaling.

epileptogenesis, with excess synchronization underlying seizure activity of neurons linked to various calcium signaling pathways (Steinlein, 2014). The rise in intracellular calcium levels upon synaptic activity triggers the activation of several kinases critical for the induction and maintenance of long-term potentiation (LTP) (Moriguchi et al., 2018), including CAMKII, CAMKIV, PKA, and PKC—all of which are downregulated in HSF. *NCKX3*, a Na^+/Ca^{2+} exchanger that plays a critical role in mediating calcium homeostasis underlying synaptic transmission (Moriguchi et al., 2018), was also downregulated in HSF (FC: −4.8).

cAMP-responsive element binding (CREB)-dependent transcription plays an important role in the maintenance of LTP and long-term memory formation in the healthy brain (*via* phosphorylation by CAMKIV) (Lakhina et al., 2015); however, in the context of epilepsy, CREB-dependent transcription contributes to increased seizures (Beaumont et al., 2012; Zhu et al., 2015). This highlights the "double-edged sword" of deactivating these signaling pathways in patients with TLE. Another HSF deactivated pathway intimately related to calcium and CREB signaling is Dopamine-DARPP32 Feedback in cAMP Signaling (Fig. 3). Deactivation of this pathway may activate a series of signaling cascades that are important in regulating neuronal excitability (Bozzi et al., 2011). If similar to results in DARPP-32 knockout mice, deactivation may have a seizure suppressive effect (O'Sullivan et al., 2008). On the other hand, deactivation of DARPP32 may also prevent the activation of key IEGs like c-fos, induction of which results in activation of a wide variety of neuron-specific genes that play a role in neuronal plasticity (Minatohara et al., 2015). Interestingly, both synaptic long-term depression (LTD) and LTP are also HSF-deactivated pathways (Fig. 4).

Perhaps a stronger case can be made that the deactivation of Opioid Signaling in HSF is a harbinger of higher seizure frequencies. Several studies underscore the conclusion that endogenous dynorphin, mediated *via* the kappa opioid receptor, is as an anticonvulsant and an antiepileptogenic agent (Burtscher and Schwarzer, 2017; Loacker et al., 2007). The modulation of neuronal activity appears to effect a reduction in glutamate release and reduced postsynaptic hyperpolarization in glutamatergic neurons (Burtscher and Schwarzer, 2017). We also note that prodynorphin (*PDYN*) is one of seven genes in our entire set of DEGs to have opposite patterns of expression in LSF and HSF groups (FC: +2.1, −4.8, respectively). Low levels of prodynorphin in humans and mice increase the risk of epilepsy development (Gambardella et al., 2003; Kauffman et al., 2008; Loacker et al., 2007; Stogmann et al., 2002). Endogenous and exogenous opioids also exert antiepileptogenic and neuroprotective effects in animal epilepsy models (Loacker et al., 2007; Schunk et al., 2011).

4.2. Common pathways modulating seizure activity in rodent and human epilepsy

Rodent models of TLE, which employ kainic acid or pilocarpine injection to initiate seizures, reproduce several of the patterns seen in human TLE. A recent study focused on the transcription factor serum response factor (*SRF*), which is activated through MAP kinase signaling and stimulates IEG expression, as well as nerve fiber growth and guidance. Lösing et al. (2017) found that SRF deficient mice were prone to spontaneous recurrent seizures, and that *SRF* was required for IEG induction, mossy fiber sprouting and inflammation. Table 4 gives a list of Lösing et al.'s (2017) top 10 genes induced after pilocarpine injection in control mice, alongside of our DE data for the same genes. The LSF group showed increased expression in 9 of these genes and all 8 of the IEGs. Of these 10 genes, *NPAS4*, *FOSB*, *GADD45G*, *EGR2*, and *EGR4* were > 10-fold over-expressed in the LSF group relative to controls. Similar to the results for pilocarpine-injected mice, our data indicate activation of MAP kinase and ERK5 signaling pathways in both the LSF

Table 3
Rank order of the 10 most significantly enriched Reactome pathways among differentially expressed genes.

Reactome Pathway	HSF*	LSF*	Mirza et al. (2015)
Signal Transduction			
Signaling by GPCR			1
GPCR downstream signaling			2
G-alpha-I signaling events			9
Visual phototransduction	4		
GPCR Ligand binding			4
Class A/1 rhodopsi-like receptors			5
Peptide ligand binding receptors			8
Neuronal System	1		6
Transmission across chemical synapses	2		7
Neurotransmitter receptors & postsynaptic signal transmission	3		
Protein-Protein interactions at synapses	9		
Potassium channels			
Voltage-gated potassium channels	10		
Transport of Small Molecules			3
SLC-mediated transmembrane transport		7	10
Immune System			
Cytokine Signaling		6	
Signaling by Interleukins		1	
Interleukin-10 signaling			
Interleukin-4 and interleukin-13 signaling		4	
Gene Expression (Transcription)		2	
RNA Polymerase II Transcription		5	
Generic Transcription Pathway		3	
Disease			
Infectious Disease			
Influenza infection	5		
Diseases of signal transduction		8	
Cellular Responses to External Stimuli		10	
Cellular Responses to Stress		9	
Metabolism			
Metaboilsm of Viatmins and Cofactors	7		
Extracellular Matrix Organization	6		
Muscle Contraction			
Cardiac conduction			
Phase 0 rapid depolarization	8		

* Rank is based on FDR p-value.

Table 4
Comparison with Lösing et al.'s[1] top 10 upregulated genes.

Locus	LSF	HSF	LSF/HSF	Fold-change in Lösing
NPAS4[2]	32.3	ns	inf	56.0
FOS[2]	2.8	ns	inf	41.2
FOSB[2]	24.8	9.1	2.7	39.3
CYR61[2]	4.7	2.8	1.7	23.2
GADD45G[2]	22.1	11.1	2.0	17.8
EGR2[2]	10.4	6.3	1.7	16.2
BTG2	3.5	2.6	1.3	15.6
ATF3[2]	3.6	ns	inf	13.7
EGR4[2]	10.1	ns	inf	13.6
THBS1	ns	ns	na	13.6

[1]See Fig. 2 in Lösing et al. (2017).
[2]Immediate Early Gene (IEG).

and HSF groups (Table 2, Fig. 4). Interestingly, CREB signaling was the top ranked transcription factor identified in their overrepresentation analysis of transcription factor binding sites (Lösing et al., 2017). Together these largely overlapping patterns support the hypothesis that downstream targets of SRF play a role in modulating response to seizures in both rodents and humans. Our RT-PCR results confirm that *SRF* is more highly expressed in LSF *versus* HSF (FC: 1.3) (Fig. 2E); however, we are not able to determine whether LSF expression is upregulated relative to controls. Therefore, it is not clear whether our data point to SRF as a key regulatory step. In sum, the emerging picture suggests that a core set of genes (*e.g.*, typical IEGs) is induced in both rodent seizure models and human TLE patients (Beaumont et al., 2012; Lösing et al., 2017).

4.3. Synaptic scaling: a key pathway for preserving higher seizure threshold?

The similarity between rodent and human studies suggests conservation of regulatory relationships among orthologous target genes in response to chronic seizures, underscoring the utility of mouse models of TLE. One of the genes in the SRF pathway that shows the largest difference in transcript abundance in the LSF *versus* HSF group is Neuronal PAS domain protein 4 (*NPAS4*) (FC: +32.3). NPAS4 is among the most rapidly induced IEGs, is expressed only in neurons, and is selectively induced by neuronal activity (Sun and Lin, 2016). It is also involved in activity-dependent synaptic modulation in both excitatory and inhibitory neurons, and regulates the expression of a large number of activity-regulated genes that mediate diverse effects on synapses (Spiegel et al., 2014). Using a mouse model based on pentylenetetrazol (PTZ)-induced kindling, Shan et al. (2018) showed that activation of the Npas4 signaling pathway after convulsive seizures plays a crucial role in intrinsic homeostatic scaling during epileptogenesis. They also showed that Npas4 controlled the homeostatic scaling capacity of hippocampal neurons through the induction of Homer1a, which regulates the surface expression of the α-amino-3-hydroxy-5-methyl-4-isoxazolepropionic acid receptor (AMPAR) GluA1 subunit, providing a molecular link between excessive neuronal hyperexcitability and the regulation of homeostatic scaling for controlling epilepsy (Shan et al., 2018). The EVH1-binding domain of Homer1 binds to Shank, group I metabotropic glutamate receptors (mGluR1/5), inositol-1,4,5-triphosphate (IP3) receptors, and ryanodine receptors (Shiraishi-Yamaguchi and Furuichi, 2007). Our results show differential expression of all of these systems, with up-regulation of *SHANK1* (FC: +3.9) and *GRM4* (FC: +3.4) in the LSF group, and down-regulation of *GRIA1* (FC: −6.3), *ITPR1* (FC: −3.5), *GRM1* (FC: −7.3), *GRM2* (FC: −3.6), *GRM5* (FC: −3.1), *RYR2* (FC: −4.0) and *RYR3* (FC: −2.2) in the HSF group (Fig. 5). Homeostatic adaptation is associated with alterations in postsynaptic AMPAR expression at excitatory synapses, which occurs through the removal and dephosphorylating of synaptic AMPARs (Seeburg and Sheng, 2008; Sun and Turrigiano, 2011; Turrigiano, 2008). This process is mediated by alterations in the signaling of protein kinase A and mGluR1/5 (Cavarsan et al., 2012; Diering et al., 2017).

Previous rodent experiments using cultured neuronal cells have shown that when the voltage-gated sodium channel blocker tetrodotoxin (TTX) is used to block activity for a short period, there is an accumulation of AMPARs at synapses, which correlates with increases in AMPAR-mediated miniature excitatory postsynaptic current (mEPSC) amplitude (known as “scaling up”). On the other hand, incubating neurons in the $GABA_A$ receptor antagonist bicuculin (BIC) mimics neural hypexcitability and leads to decreased synaptic AMPAR content and AMPAR-mEPSC amplitude (known as “scaling down”) (Ju et al., 2004; O’Brien et al., 1998; Thiagarajan et al., 2005; Turrigiano, 2008; Wierenga et al., 2005). The long-term effect of the AMPAR accumulation or loss suggested that the process is transcription dependent (Ibata et al., 2008). The upstream regulator analysis tool in IPA implicated bicuculline as a significant upstream effector molecule only in the LSF group (z-score: 4.0, p-value: 1.1×10^{-15}), consistent with a gene expression profile that is capable of scaling down in the face of chronic neuronal excitation.

A plausible explanation for the much lower seizure frequencies in the LSF group follows from this seminal work showing a link between synaptic scaling of excitatory synaptic transmission and regulation of the excitation/inhibition balance (Chowdhury and Hell, 2018). Fig. 5 summarizes our results in a model of synaptic scaling through AMPA receptor recycling in the postsynaptic compartment of excitatory neurons. This model features two phases, an initial transcriptional response

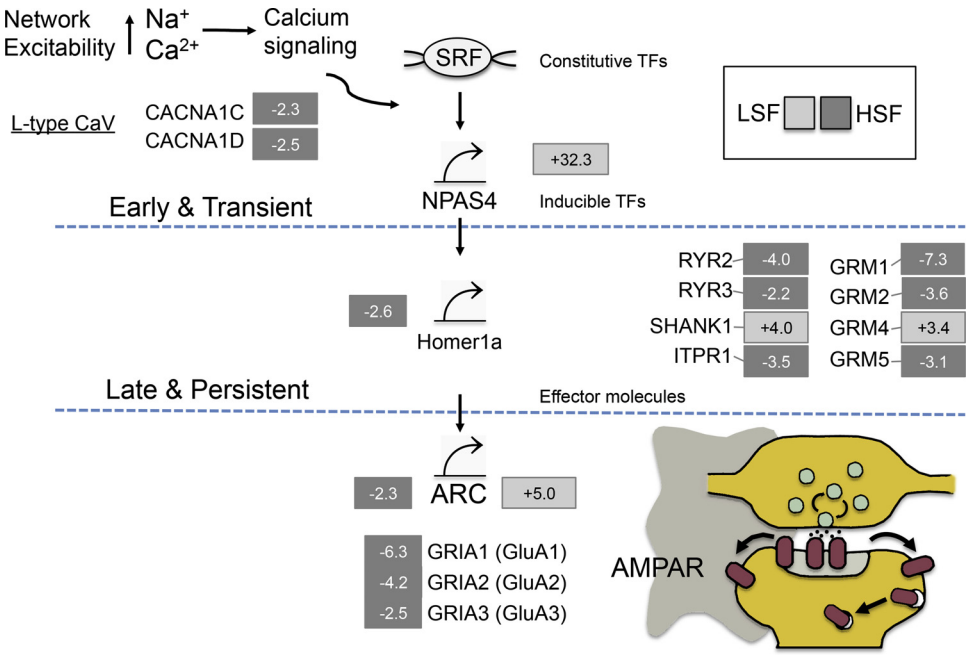

Fig. 5. A model of synaptic downscaling through AMPA receptor recycling in the post-synaptic compartment of excitatory neurons. Neuronal depolarization leads to increased intracellular levels of the second messenger Ca^{2+} (*via* NMDA receptors and L-type calcium channels) and activation of intracellular kinases. SRF, a constitutively expressed transcription factor (TF), is rapidly activated and, in turn, induces the expression of NPAS4 and other inducible TFs and effector molecules that initiate a second wave of gene expression. Late and persistent processes acting through Activity Regulated Cytoskeleton Associated Protein (ARC) regulate the surface expression of the AMPAR GluA1 subunit (*GRIA1*) by endocytosis or by lateral diffusion from synaptic to extrasynaptic sites, leading to a reduction in AMPAR-mediated synaptic strength (scaling down). Numbers in boxes represent fold-change for the particular DEG. The image in the lower right is a schematic representing presynaptic and postsynaptic terminals (yellow), AMPA receptors (maroon ovals), intracellular receptor pools, and glial cells (shown in gray) (image after Pozo and Goda, 2010).

resulting in expression of transcription factors encoding IEGs, followed by a second delayed gene expression wave resulting in expression of further effector genes (Lösing et al., 2017). A key end-point regulating synaptic homeostasis is the IEG gene, activity-regulated cytoskeleton-associated protein (*ARC*). ARC protein associates with the post-synaptic density and plays a critical role in AMPA receptor endocytosis, thereby contributing to downregulation of synaptic efficacy at excitatory synapses (Chowdhury et al., 2006; Rial Verde et al., 2006; Shepherd et al., 2006; Steward et al., 2014).

Interestingly, neuronal pentraxin-1 (*NPTX1*), a gene that was found to be necessary for the TTX-induced scaling up effect in mouse cortical neurons (Schaukowitch et al., 2017), as well as it's receptor (*NPTXR*), are downregulated in the HSF group (FC: −2.7 and −7.3, respectively). The *NPTX1* gene has a known role in promoting the clustering of AMPARs (Sia et al., 2007; Xu et al., 2003). NPTX1 induction is mediated by calcium influx through T-type voltage-gated calcium channels, as well as the transcription factors, SRF and ELK1 (Schaukowitch et al., 2017). The T-type calcium channel genes, *CACNA1H* and *CACNA1I* are downregulated in the HSF (FC: −2.4 and −3.2, respectively) (Fig. 5), while a third T-type channel gene, *CACNA1G*, is upregulated in the LSF group (FC: +3.3). Both GluA1 and GluA2 are important for scaling up and yet are downregulated in HSF (Fig. 5), as is the glutamate receptor-interacting protein (*GRIP1*) (HSF FC: −2.5), which interacts with the cytosolic GluA2 C-terminus (Chowdhury and Hell, 2018). Additional evidence that HSF may have diminished capacity to scale up comes from results showing that up-regulation of AKAP5-anchored PKA activity drives scaling up (Chowdhury and Hell, 2018); yet we find that both regulatory subunits of PKA (*PRKAR1B* and *PRKAR2B*) are downregulated in HSF, as is *AKAP5* (FC: −4.0).

While HSF is distinguished from LSF in terms of *NPAS4* upregulation and associated alterations on the pathway shown in Fig. 5, there are additional indications in our data that HSF has lost the capacity to scale down. For example, two catalytic subunits of calcineurin A (*PPP3CA* and *PPP3CB* are downregulated in HSF (FC: −4.3 and −2.3, respectively). Dephosphorylation of Ser845 by calcineurin in bicuculline-induced downscaling accompanies endocytosis of AMPARs in cultured neurons. Moreover, two L-type calcium channels *CACNA1C* and *CACNA1D* that participate in calcium signaling cascades required for NPAS4 activation (Chen et al., 2017) are also downregulated in HSF (Fig. 5). Together these results are consistent with hypothesis that the HSF group has diminished capacity in both scaling up and scaling down.

4.4. Systematic down-regulation of pathways in the HSF group: remodeling by gene regulation or by neuronal loss?

Upon initial consideration it seems counterintuitive to discover so many HSF deactivated pathways, many of which are thought to promote seizures and epileptogenesis (Table 2). One explanation is that compensatory changes in response to frequent seizures had a cascading effect on gene expression in many downstream pathways. It is well known that fluctuations in neuronal activity that induce adaptive changes in gene expression in the neurotypical brain can be maladaptive in the context of epilepsy (Scharfman, 2015; Varvel et al., 2015). For example, synaptic release of glutamate leading to excessive NMDA receptor activation and Ca^{2+} influx would typically induce scaling down *via* a reduced surface insertion of GluA1 of AMPA receptors at synaptic sites. If the scaling down process is impaired there may be other compensatory mechanisms (*e.g.*, homeostatic reduction in CAMKII activity (McNamara et al., 2006)) that would have consequences for gene expression in additional pathways. Indeed, several studies have shown that compensatory mechanisms can act through switches in GPCR subunit utilization (Narla et al., 2016; Warren et al., 2017; Watts and Neve, 2005).

Neuronal loss represents an alternative mechanism that does not depend on numerous changes in gene regulation across multiple pathways. For example, selective neuronal cell death in hippocampal sclerosis is often observed in subregions CA1, CA3 and CA4, while granule cells of the dentate gyrus are usually spared (Schmeiser et al., 2017). Support for this model comes from recent work with the pilocarpine model of TLE in rats, in which a negative correlation was found between seizure frequency and the total number of neuronal cells throughout the life of rats with epilepsy (Lopim et al., 2016). In attempting to explain a similar phenomenon of widespread down-regulation of synaptic genes across different brain regions in aging and Alzheimer's patients, Berchtold et al. (2013) concluded that the decline in gene expression in AD patients could be due to the loss of neurons and synapses in the hippocampus, while synaptic remodeling by changes in gene expression was a more likely explanation for

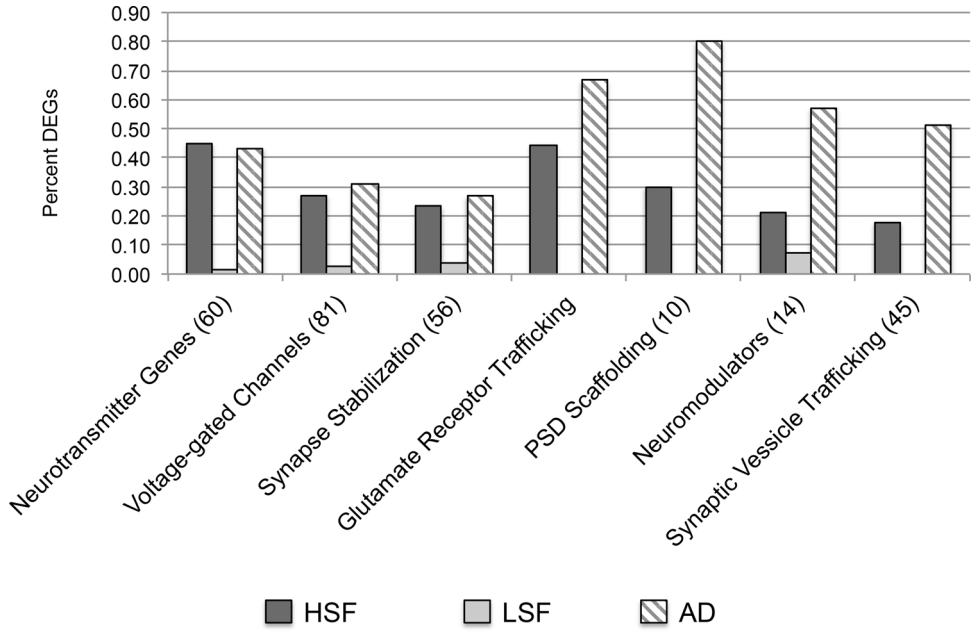

Fig. 6. Percentage of differentially expressed genes in seven gene sets related to synaptic transmission. Percentages are calculated based on the number of DEGs in each cohort (HSF, LSF and Alzheimer) relative to the total number of genes in each of 7 gene sets as described in Berchtold et al. (2013) (see their tables S2-S8).

neocortical region downregulation in the aging patients. Their microarray-based study of synaptic gene expression identified many of the same genes and pathways in the AD patients as seen here exclusively in the HSF group, with DEGs enriched in gene sets related to neurotransmitter, voltage-gated channels, and synapse stabilization pathways (Berchtold et al., 2013) (Fig. 6).

5. Limitations

Despite these promising results, there are at least three limitations to note. First, we performed differential expression analysis on a relatively small cohort (*i.e.*, with only 3 individuals per seizure frequency group). The small sample sizes reflect the number of resections performed at our center for which we could identify individuals with very low and high pre-surgery seizure frequency. We also wanted to control for sex as female-male differences in gene expression and splicing are widespread in adult human brain and involve ~2.6% of all expressed genes (Trabzuni et al., 2013). However, as shown by Schurch et al. (2016), biological replicates of ≥3 yield a true positive rate greater than 85% using the methods we have employed here. Indeed, all 11 of the genes we chose to validate using qRT-PCR gave results that were quite similar to those based on RNA-seq. Moreover, rather than relying on any single transcript, we focused on pathways that were enriched by dozens of DEGs in our analysis, thereby reducing our false positive rate at the level of pathways. The second limitation is the lack of suitable control tissue. We relied on post-mortem hippocampal tissue for most of our comparisons. However, when we performed differential expression analysis comparing LSF directly with HSF, we also noted a very large number of DEGs that showed a similar pattern of lower transcript abundance in the HSF, independent of comparisons with post-mortem controls (Fig. S1).

To further validate our RNA-seq results, we performed analyses comparing the same number of individuals in groups with a similar mean seizure frequency, and looked at expression patterns for genes that are differentially expressed in different brain regions to confirm that the DEGs primarily are hippocampal in origin. Because brain tissue is usually resected at the end-stage of the disease it is difficult to infer the initial steps in the process of epileptogenesis when using human hippocampal specimens (Korotkov et al., 2017). Indeed, our patients had seizures for an average of > 20 years before surgery. On the other hand, we find consistency with both other human studies and those utilizing animal models that have the ability to examine earlier stages of epileptogenesis.

Despite these consistencies, it is challenging to infer cause and effect in human studies. It is also important to note that the results presented here represent only a single snapshot in time of gene expression levels in a single region of the brain. Many TFs act as both a repressor and an activator under different conditions at different promoters, and as such the function of the IEG, NPAS4, under different conditions throughout the brain will be an important area of future investigation. An additional point of caution comes from the fact that the low and high seizure frequency patients will have had different probabilities of experiencing a seizure just prior to surgery. Finally, our results do not distinguish the cause of the systematic downregulation seen in the HSF group. Further work is needed to test the predictions of the hypotheses that downregulation is a result of remodeling by neuronal loss, or synaptic reprogramming (*i.e.*, by small changes in genes on many pathways).

Acknowledgments

This research was supported by RO1MH065151 (Yuri Persidsky, Temple University) (HCS 04-42), NIH subcontract from Temple University to University of Arizona; the Department of Surgery 2016 Faculty Seed Grant, University of Arizona College of Medicine; and the 2016 University of Arizona Health Sciences Clinical Research Pilot Program Award (UAHS-CRPA). We thank Jon Gallina-Mehlman and Joseph Still for excellent technical assistance, and the patients who contributed their specimens to this study.

Appendix A. Supplementary data

Supplementary material related to this article can be found, in the online version, at doi:https://doi.org/10.1016/j.eplepsyres.2019.05.013.

References

Anders, S., Pyl, P.T., Huber, W., 2015. HTSeq–a Python framework to work with high-throughput sequencing data. Bioinformatics 31, 166–169.

Asadi-Pooya, A.A., Stewart, G.R., Abrams, D.J., Sharan, A., 2017. Prevalence and incidence of drug-resistant mesial temporal lobe epilepsy in the United States. World Neurosurg. 99, 662–666.
Beaumont, T.L., Yao, B., Shah, A., Kapatos, G., Loeb, J.A., 2012. Layer-specific CREB target gene induction in human neocortical epilepsy. J. Neurosci. 32, 14389–14401.
Berchtold, N.C., Coleman, P.D., Cribbs, D.H., Rogers, J., Gillen, D.L., Cotman, C.W., 2013. Synaptic genes are extensively downregulated across multiple brain regions in normal human aging and Alzheimer's disease. Neurobiol. Aging 34, 1653–1661.
Bozzi, Y., Dunleavy, M., Henshall, D.C., 2011. Cell signaling underlying epileptic behavior. Front. Behav. Neurosci. 5, 45.
Burtscher, J., Schwarzer, C., 2017. The opioid system in temporal lobe epilepsy: functional role and therapeutic potential. Front. Mol. Neurosci. 10, 245.
Cavarsan, C.F., Tescarollo, F., Tesone-Coelho, C., Morais, R.L., Motta, F.L., Blanco, M.M., Mello, L.E., 2012. Pilocarpine-induced status epilepticus increases Homer1a and changes mGluR5 expression. Epilepsy Res. 101, 253–260.
Chen, L.F., Zhou, A.S., West, A.E., 2017. Transcribing the connectome: roles for transcription factors and chromatin regulators in activity-dependent synapse development. J. Neurophysiol. 118, 755–770.
Chowdhury, D., Hell, J.W., 2018. Homeostatic synaptic scaling: molecular regulators of synaptic AMPA-type glutamate receptors. F1000Res 7, 234.
Chowdhury, S., Shepherd, J.D., Okuno, H., Lyford, G., Petralia, R.S., Plath, N., Kuhl, D., Huganir, R.L., Worley, P.F., 2006. Arc/Arg3.1 interacts with the endocytic machinery to regulate AMPA receptor trafficking. Neuron 52, 445–459.
Diering, G.H., Nirujogi, R.S., Roth, R.H., Worley, P.F., Pandey, A., Huganir, R.L., 2017. Homer1a drives homeostatic scaling-down of excitatory synapses during sleep. Science 355, 511–515.
Dixit, A.B., Banerjee, J., Srivastava, A., Tripathi, M., Sarkar, C., Kakkar, A., Jain, M., Chandra, P.S., 2016. RNA-seq analysis of hippocampal tissues reveals novel candidate genes for drug refractory epilepsy in patients with MTLE-HS. Genomics 107, 178–188.
Dobin, A., Davis, C.A., Schlesinger, F., Drenkow, J., Zaleski, C., Jha, S., Batut, P., Chaisson, M., Gingeras, T.R., 2013. STAR: ultrafast universal RNA-seq aligner. Bioinformatics 29, 15–21.
Englot, D.J., Rutkowski, M.J., Ivan, M.E., Sun, P.P., Kuperman, R.A., Chang, E.F., Gupta, N., Sullivan, J.E., Auguste, K.I., 2013. Effects of temporal lobectomy on consciousness-impairing and consciousness-sparing seizures in children. Childs Nerv. Syst. 29, 1915–1922.
Fiala, M., Avagyan, H., Merino, J.J., Bernas, M., Valdivia, J., Espinosa-Jeffrey, A., Witte, M., Weinand, M., 2013. Chemotactic and mitogenic stimuli of neuronal apoptosis in patients with medically intractable temporal lobe epilepsy. Pathophysiology 20, 59–69.
Gambardella, A., Manna, I., Labate, A., Chifari, R., Serra, P., La Russa, A., LePiane, E., Cittadella, R., Andreoli, V., Sasanelli, F., Zappia, M., Aguglia, U., Quattrone, A., 2003. Prodynorphin gene promoter polymorphism and temporal lobe epilepsy. Epilepsia 44, 1255–1256.
Gowers, W.R., 1881. Epilepsy and Other Chronic Convulsive Disorders: Their Causes, Symptoms and Treatment. J&A Churchill, London.
Griffin, N.G., Wang, Y., Hulette, C.M., Halvorsen, M., Cronin, K.D., Walley, N.M., Haglund, M.M., Radtke, R.A., Skene, J.H., Sinha, S.R., Heinzen, E.L., 2016. Differential gene expression in dentate granule cells in mesial temporal lobe epilepsy with and without hippocampal sclerosis. Epilepsia 57, 376–385.
Hansen, K.F., Sakamoto, K., Pelz, C., Impey, S., Obrietan, K., 2014. Profiling status epilepticus-induced changes in hippocampal RNA expression using high-throughput RNA sequencing. Sci. Rep. 4, 6930.
Hwang, T., Park, C.K., Leung, A.K., Gao, Y., Hyde, T.M., Kleinman, J.E., Rajpurohit, A., Tao, R., Shin, J.H., Weinberger, D.R., 2016. Dynamic regulation of RNA editing in human brain development and disease. Nat. Neurosci. 19, 1093–1099.
Ibata, K., Sun, Q., Turrigiano, G.G., 2008. Rapid synaptic scaling induced by changes in postsynaptic firing. Neuron 57, 819–826.
Ju, W., Morishita, W., Tsui, J., Gaietta, G., Deerinck, T.J., Adams, S.R., Garner, C.C., Tsien, R.Y., Ellisman, M.H., Malenka, R.C., 2004. Activity-dependent regulation of dendritic synthesis and trafficking of AMPA receptors. Nat. Neurosci. 7, 244–253.
Kandratavicius, L., Balista, P.A., Lopes-Aguiar, C., Ruggiero, R.N., Umeoka, E.H., Garcia-Cairasco, N., Bueno-Junior, L.S., Leite, J.P., 2014. Animal models of epilepsy: use and limitations. Neuropsychiatr. Dis. Treat. 10, 1693–1705.
Kang, H.J., Kawasawa, Y.I., Cheng, F., Zhu, Y., Xu, X., Li, M., Sousa, A.M., Pletikos, M., Meyer, K.A., Sedmak, G., Guennel, T., Shin, Y., Johnson, M.B., Krsnik, Z., Mayer, S., Fertuzinhos, S., Umlauf, S., Lisgo, S.N., Vortmeyer, A., Weinberger, D.R., Mane, S., Hyde, T.M., Huttner, A., Reimers, M., Kleinman, J.E., Sestan, N., 2011. Spatio-temporal transcriptome of the human brain. Nature 478, 483–489.
Kauffman, M.A., Consalvo, D., Gonzalez, M.D., Kochen, S., 2008. Transcriptionally less active prodynorphin promoter alleles are associated with temporal lobe epilepsy: a case-control study and meta-analysis. Dis. Markers 24, 135–140.
Korotkov, A., Mills, J.D., Gorter, J.A., van Vliet, E.A., Aronica, E., 2017. Systematic review and meta-analysis of differentially expressed miRNAs in experimental and human temporal lobe epilepsy. Sci. Rep. 7, 11592.
Kramer, A., Green, J., Pollard Jr, J., Tugendreich, S., 2014. Causal analysis approaches in ingenuity pathway analysis. Bioinformatics 30, 523–530.
Lakhina, V., Arey, R.N., Kaletsky, R., Kauffman, A., Stein, G., Keyes, W., Xu, D., Murphy, C.T., 2015. Genome-wide functional analysis of CREB/long-term memory-dependent transcription reveals distinct basal and memory gene expression programs. Neuron 85, 330–345.
Langfelder, P., Horvath, S., 2008. WGCNA: an R package for weighted correlation network analysis. BMC Bioinf. 9, 559–571.
Laxer, K.D., Trinka, E., Hirsch, L.J., Cendes, F., Langfitt, J., Delanty, N., Resnick, T., Benbadis, S.R., 2014. The consequences of refractory epilepsy and its treatment. Epilepsy Behav. 37, 59–70.
Li, X.W., Yang, F., Wang, Y.G., Wang, J.C., Ma, L., Jiang, W., 2013. Brain recruitment of dendritic cells following Li-pilocarpine induced status epilepticus in adult rats. Brain Res. Bull. 91, 8–13.
Livak, K.J., Schmittgen, T.D., 2001. Analysis of relative gene expression data using real-time quantitative PCR and the 2(-Delta Delta C(T)) Method. Methods 25, 402–408.
Loacker, S., Sayyah, M., Wittmann, W., Herzog, H., Schwarzer, C., 2007. Endogenous dynorphin in epileptogenesis and epilepsy: anticonvulsant net effect via kappa opioid receptors. Brain 130, 1017–1028.
Lopim, G.M., Vannucci Campos, D., Gomes da Silva, S., de Almeida, A.A., Lent, R., Cavalheiro, E.A., Arida, R.M., 2016. Relationship between seizure frequency and number of neuronal and non-neuronal cells in the hippocampus throughout the life of rats with epilepsy. Brain Res. 1634, 179–186.
Lösing, P., Niturad, C.E., Harrer, M., Reckendorf, C.M.Z., Schatz, T., Sinske, D., Lerche, H., Maljevic, S., Knoll, B., 2017. SRF modulates seizure occurrence, activity induced gene transcription and hippocampal circuit reorganization in the mouse pilocarpine epilepsy model. Mol. Brain 10, 30.
Love, M.I., Huber, W., Anders, S., 2014. Moderated estimation of fold change and dispersion for RNA-seq data with DESeq2. Genome Biol. 15, 550.
Malaiyan, J., Ramanan, P.V., Subramaniam, D., Menon, T., 2016. Analysis of serum Th1/Th2 cytokine levels in patients with acute mumps infection. J. Glob. Infect. Dis. 8, 87–92.
McGraw, C.M., Ward, C.S., Samaco, R.C., 2017. Genetic rodent models of brain disorders: perspectives on experimental approaches and therapeutic strategies. Am. J. Med. Genet. C Semin. Med. Genet. 175, 368–379.
McNamara, J.O., Huang, Y.Z., Leonard, A.S., 2006. Molecular signaling mechanisms underlying epileptogenesis. Sci. STKE 2006 re12.
Merico, D., Isserlin, R., Stueker, O., Emili, A., Bader, G.D., 2010. Enrichment map: a network-based method for gene-set enrichment visualization and interpretation. PLoS One 5, e13984.
Minatohara, K., Akiyoshi, M., Okuno, H., 2015. Role of immediate-early genes in synaptic plasticity and neuronal ensembles underlying the memory trace. Front. Mol. Neurosci. 8, 78.
Mirza, N., Appleton, R., Burn, S., Carr, D., Crooks, D., du Plessis, D., Duncan, R., Farah, J.O., Josan, V., Miyajima, F., Mohanraj, R., Shukralla, A., Sills, G.J., Marson, A.G., Pirmohamed, M., 2015. Identifying the biological pathways underlying human focal epilepsy: from complexity to coherence to centrality. Hum. Mol. Genet. 24, 4306–4316.
Moriguchi, S., Kita, S., Yabuki, Y., Inagaki, R., Izumi, H., Sasaki, Y., Tagashira, H., Horie, K., Takeda, J., Iwamoto, T., Fukunaga, K., 2018. Reduced CaM kinase II and CaM kinase IV activities underlie cognitive deficits in NCKX2 heterozygous mice. Mol. Neurobiol. 55, 3889–3900.
Narla, C., Scidmore, T., Jeong, J., Everest, M., Chidiac, P., Poulter, M.O., 2016. A switch in G protein coupling for type 1 corticotropin-releasing factor receptors promotes excitability in epileptic brains. Sci. Signal. 9 ra60.
Ngugi, A.K., Bottomley, C., Kleinschmidt, I., Sander, J.W., Newton, C.R., 2010. Estimation of the burden of active and life-time epilepsy: a meta-analytic approach. Epilepsia 51, 883–890.
O'Brien, R.J., Kamboj, S., Ehlers, M.D., Rosen, K.R., Fischbach, G.D., Huganir, R.L., 1998. Activity-dependent modulation of synaptic AMPA receptor accumulation. Neuron 21, 1067–1078.
O'Sullivan, G.J., Dunleavy, M., Hakansson, K., Clementi, M., Kinsella, A., Croke, D.T., Drago, J., Fienberg, A.A., Greengard, P., Sibley, D.R., Fisone, G., Henshall, D.C., Waddington, J.L., 2008. Dopamine D1 vs D5 receptor-dependent induction of seizures in relation to DARPP-32, ERK1/2 and GluR1-AMPA signalling. Neuropharmacology 54, 1051–1061.
Pozo, K., Goda, Y., 2010. Unraveling mechanisms of homeostatic synaptic plasticity. Neuron 66, 337–351.
Rial Verde, E.M., Lee-Osbourne, J., Worley, P.F., Malinow, R., Cline, H.T., 2006. Increased expression of the immediate-early gene arc/arg3.1 reduces AMPA receptor-mediated synaptic transmission. Neuron 52, 461–474.
Robinson, M.D., McCarthy, D.J., Smyth, G.K., 2010. edgeR: a Bioconductor package for differential expression analysis of digital gene expression data. Bioinformatics 26, 139–140.
Scharfman, H.E., 2015. Epilepsy. In: Zigmond, M.J., Rowland, L.P., Coyle, J.T. (Eds.), Neurobiology of Brain Disorders: Biological Basis of Neurological and Psychiatric Disorders. Academic Press (Elsevier Inc.), Boston, pp. 236–261.
Schaukowitch, K., Reese, A.L., Kim, S.K., Kilaru, G., Joo, J.Y., Kavalali, E.T., Kim, T.K., 2017. An intrinsic transcriptional program underlying synaptic scaling during activity suppression. Cell Rep. 18, 1512–1526.
Schmeiser, B., Zentner, J., Prinz, M., Brandt, A., Freiman, T.M., 2017. Extent of mossy fiber sprouting in patients with mesiotemporal lobe epilepsy correlates with neuronal cell loss and granule cell dispersion. Epilepsy Res. 129, 51–58.
Schunk, E., Aigner, C., Stefanova, N., Wenning, G., Herzog, H., Schwarzer, C., 2011. Kappa opioid receptor activation blocks progressive neurodegeneration after kainic acid injection. Hippocampus 21, 1010–1020.
Schurch, N.J., Schofield, P., Gierlinski, M., Cole, C., Sherstnev, A., Singh, V., Wrobel, N., Gharbi, K., Simpson, G.G., Owen-Hughes, T., Blaxter, M., Barton, G.J., 2016. How many biological replicates are needed in an RNA-seq experiment and which differential expression tool should you use? RNA 22, 839–851.
Seeburg, D.P., Sheng, M., 2008. Activity-induced Polo-like kinase 2 is required for homeostatic plasticity of hippocampal neurons during epileptiform activity. J. Neurosci. 28, 6583–6591.
Shan, W., Nagai, T., Tanaka, M., Itoh, N., Furukawa-Hibi, Y., Nabeshima, T., Sokabe, M., Yamada, K., 2018. Neuronal PAS domain protein 4 (Npas4) controls neuronal homeostasis in pentylenetetrazole-induced epilepsy through the induction of

Homer1a. J. Neurochem. 145, 19–33.
Shepherd, J.D., Rumbaugh, G., Wu, J., Chowdhury, S., Plath, N., Kuhl, D., Huganir, R.L., Worley, P.F., 2006. Arc/Arg3.1 mediates homeostatic synaptic scaling of AMPA receptors. Neuron 52, 475–484.
Shiraishi-Yamaguchi, Y., Furuichi, T., 2007. The homer family proteins. Genome Biol. 8, 206.
Sia, G.M., Beique, J.C., Rumbaugh, G., Cho, R., Worley, P.F., Huganir, R.L., 2007. Interaction of the N-terminal domain of the AMPA receptor GluR4 subunit with the neuronal pentraxin NP1 mediates GluR4 synaptic recruitment. Neuron 55, 87–102.
Spiegel, I., Mardinly, A.R., Gabel, H.W., Bazinet, J.E., Couch, C.H., Tzeng, C.P., Harmin, D.A., Greenberg, M.E., 2014. Npas4 regulates excitatory-inhibitory balance within neural circuits through cell-type-specific gene programs. Cell 157, 1216–1229.
Steinlein, O.K., 2014. Calcium signaling and epilepsy. Cell Tissue Res. 357, 385–393.
Steward, O., Farris, S., Pirbhoy, P.S., Darnell, J., Driesche, S.J., 2014. Localization and local translation of Arc/Arg3.1 mRNA at synapses: some observations and paradoxes. Front. Mol. Neurosci. 7, 101.
Stogmann, E., Zimprich, A., Baumgartner, C., Aull-Watschinger, S., Hollt, V., Zimprich, F., 2002. A functional polymorphism in the prodynorphin gene promotor is associated with temporal lobe epilepsy. Ann. Neurol. 51, 260–263.
Subramanian, A., Tamayo, P., Mootha, V.K., Mukherjee, S., Ebert, B.L., Gillette, M.A., Paulovich, A., Pomeroy, S.L., Golub, T.R., Lander, E.S., Mesirov, J.P., 2005. Gene set enrichment analysis: a knowledge-based approach for interpreting genome-wide expression profiles. Proc Natl Acad Sci U S A 102, 15545–15550.
Sun, Q., Turrigiano, G.G., 2011. PSD-95 and PSD-93 play critical but distinct roles in synaptic scaling up and down. J. Neurosci. 31, 6800–6808.
Sun, X., Lin, Y., 2016. Npas4: linking neuronal activity to memory. Trends Neurosci. 39, 264–275.
Tellez-Zenteno, J.F., Hernandez-Ronquillo, L., 2012. A review of the epidemiology of temporal lobe epilepsy. Epilepsy Res. Treat. 2012, 630853.
Thiagarajan, T.C., Lindskog, M., Tsien, R.W., 2005. Adaptation to synaptic inactivity in hippocampal neurons. Neuron 47, 725–737.
Trabzuni, D., Ramasamy, A., Imran, S., Walker, R., Smith, C., Weale, M.E., Hardy, J., Ryten, M., North American Brain Expression, 2013. Widespread sex differences in gene expression and splicing in the adult human brain. Nat. Commun. 4, 2771.
Turrigiano, G.G., 2008. The self-tuning neuron: synaptic scaling of excitatory synapses. Cell 135, 422–435.
Varvel, N.H., Jiang, J., Dingledine, R., 2015. Candidate drug targets for prevention or modification of epilepsy. Annu. Rev. Pharmacol. Toxicol. 55, 229–247.
Vezzani, A., Fujinami, R.S., White, H.S., Preux, P.M., Blumcke, I., Sander, J.W., Loscher, W., 2016. Infections, inflammation and epilepsy. Acta Neuropathol. 131, 211–234.
Vieira, A.S., de Matos, A.H., do Canto, A.M., Rocha, C.S., Carvalho, B.S., Pascoal, V.D., Norwood, B., Bauer, S., Rosenow, F., Gilioli, R., Cendes, F., Lopes-Cendes, I., 2016. RNA sequencing reveals region-specific molecular mechanisms associated with epileptogenesis in a model of classical hippocampal sclerosis. Sci. Rep. 6, 22416.
Warren, E.B., Sillivan, S.E., Konradi, C., 2017. Receptors and second messengers in the basal ganglia. In: Steiner, H., Tseng, K. (Eds.), Handbook of Basal Ganglia Structure and Function. Elsevier.
Watts, V.J., Neve, K.A., 2005. Sensitization of adenylate cyclase by Galpha i/o-coupled receptors. Pharmacol. Ther. 106, 405–421.
Wierenga, C.J., Ibata, K., Turrigiano, G.G., 2005. Postsynaptic expression of homeostatic plasticity at neocortical synapses. J. Neurosci. 25, 2895–2905.
Xu, D., Hopf, C., Reddy, R., Cho, R.W., Guo, L., Lanahan, A., Petralia, R.S., Wenthold, R.J., O'Brien, R.J., Worley, P., 2003. Narp and NP1 form heterocomplexes that function in developmental and activity-dependent synaptic plasticity. Neuron 39, 513–528.
Zhu, X., Dubey, D., Bermudez, C., Porter, B.E., 2015. Suppressing cAMP response element-binding protein transcription shortens the duration of status epilepticus and decreases the number of spontaneous seizures in the pilocarpine model of epilepsy. Epilepsia 56, 1870–1878.